

SWE Retrieval Algorithms Based on the Parameterized Bi-Continuous DMRT Model without Priors on Grain Size or Scattering Albedo

Firoz Kanti Borah^{1,*}, Leung Tsang¹, and Edward Kim²

¹Department of Electrical Engineering and Computer Science, University of Michigan, Ann Arbor, MI 48109, USA

²NASA Goddard Space Flight Center, Greenbelt, MD, USA

ABSTRACT: In this paper, we develop two improved retrieval algorithms of snow water equivalent (SWE) based on the volume scattering snow at X (9.6 GHz) and Ku (17.2 GHz) bands. Significantly, neither algorithm requires a prior on grain size nor scattering albedo. The two algorithms are validated with 4 sets of airborne data and 3 years of tower time series measurements. The two algorithms are based on improvements of the previous algorithm published in the previous two papers [1, 2]. The physical model is the bi-continuous DMRT model, and a parametrization is carried out over a look-up table of DMRT results. The parameterized model gives the X and Ku band copolarization backscatter as a pair of equations in terms of two parameters SWE and scattering albedo at X band (ω_X). The solution space of two measurements and two parameters has been carefully studied. By directly inverting the pair of equations for, $\sigma^X(SWE, \omega_X)$ and $\sigma^{Ku}(SWE, \omega_X)$ we show that there are at most a pair of solutions which have SWE values that are far apart in most cases, facilitating identification of the correct solution. The first algorithm described in this paper, labeled algebraic algorithm, uses inversion alone and does not employ a cost function. The robustness of the no-prior approach was validated with the airborne observations, by using a prior SWE value that is intentionally far (75% different) from the true SWE. For the validation using tower-based data, time series observations from the NoSREx experiment in Sodankyla, Finland were used in which the SWE of the previous time step is used to correctly choose between the two solutions for the current time step. The second cost function-based algorithm finds the SWE and ω_X pair which minimizes the difference between the observed volume scattering $\sigma^{X,obs}$ and $\sigma^{Ku,obs}$ and the model-predicted volume scattering $\sigma^{X,mod}$ and $\sigma^{Ku,mod}$. The cost function uses prior information on SWE, also based on a time series starting with zero/low SWE. NoSREx data is used to show results from this approach. The new algorithm combined with time series eliminates the need for ancillary information of SWE and grain sizes, making the algorithm useful for level-2 products of a satellite mission.

1. INTRODUCTION

Snow water equivalent (SWE) is an important parameter of relevance for hydrological, climatological, and meteorological applications and active microwave remote sensing has great potential to monitor snow cover and retrieve SWE. X- and Ku-band radar measurements [1–6], provide a viable pathway to produce SWE information at the temporal and spatial scales necessary to advance operational environmental prediction, climate monitoring, and water resource management across the northern hemisphere. The ESA Cold Regions Hydrology High-Resolution Observatory (CoReH₂O) mission (dual-frequency X- and Ku-band; Rott et al., 2010 [3]) was a major impetus. The potential for Ku-band radar was also explored at NASA as part of the Snow and Cold Land Processes Mission (Yueh et al., 2009 [6]). A recent review paper [4] highlights the progress that was made over the past decade in understanding the physics of the X-band and Ku-band radar response to variations in SWE, snow microstructure, and snow-wet/dry state. Physically based retrieval algorithms were also developed in [4]. We developed an algorithm (Zhu et al. algorithm) in our previous two papers [1, 2] based on X and Ku band volume scattering which

was summarized in the review paper [4] Previously retrieval algorithms were mainly on passive microwaves as described by Chang and his collaborators [7–11]. Early work on modeling active remote sensing of SWE and ground measurements are in references [12–14]. Forward scattering models include QCA-DMRT [14], MEMLS [15], Bi-continuous DMRT [16, 17], and SMRT [18]. For radar backscattering remote sensing, experimental airborne and tower measurements have been used to advance understanding of the physics of radar backscatter response to snow microstructure and SWE (Lemmetyinen et al., 2018 [19]; King et al., 2018 [20]). Backscattering enhancement is an important phenomenon in active remote sensing and can apply to satellite remote sensing of snow at X and Ku bands subject to validation by more experimental measurements [17, 21–23].

The amount of volume scattering is related to the amount of SWE. Measuring volume scattering can be used to infer SWE as shown in [4]. However, the backscatter is also affected by rough soil surface scattering beneath the snowpack. The scattering from the snowpack itself (volume scattering) is controlled by the depth, density, and snow microstructure parameters such as grain size, correlation length etc.. In a dual frequency, single polarization-based retrieval, there are two mea-

* Corresponding author: Firoz Kanti Borah (firozb@umich.edu).

measurements (co-polarized X and Ku band) and several parameters of snow microstructure and roughness. Thus, it is important to develop an effective SWE retrieval algorithm based on two measurements. Historically, the primary confounding factor in SWE retrieval through volume scattering is the grain size. Even in the case of SWE or snow depth retrieval using two-channel passive measurements Kelly et al. 2003 [10] and Foster et al. 2005 [11] used a fixed grain size of 0.3 mm and a fixed density of 300 kg m^{-3} globally in their algorithm. In active measurement retrieval, Rott et al. 2010 [3], Cui et al. 2016 [24], etc. use a prior grain size. For a global SWE retrieval satellite mission, the algorithm needs to be able to retrieve SWE in real time both accurately and reliably. A common approach for SWE retrieval from radar measurements is via the use of cost functions. A cost function for retrieving SWE can be given by

$$\hat{x} = w_1 \sum_{j=1}^n \frac{1}{2\sigma_j^2} [\Phi_j(x_1, \dots, x_q) - Z_j]^2 + w_2 \sum_{i=1}^q \frac{1}{2\lambda_i^2} (x_i - \bar{x}_i)^2$$

where x_i , $i = 1, 2 \dots q$, are parameters such as SWE, grain size, and snow densities. Z_j , $j = 1, \dots n$ is the observed backscatter from the snowpack, and Φ is the forward model for the backscatter from the snow. \bar{x}_i is the prior information for parameter x_i , and the σ_j^2 and λ_i^2 are the error covariances associated with the j^{th} measurement and the i^{th} prior, respectively. In the cost function equation, n is the number of observations, and q is the number of parameters. The first term consists of a physically based model matched to remote sensing measurements and the second term is prior information and error estimates. The cost function algorithm is often criticized for the large amount of ancillary information required that may not be available on spatial and time scales for a satellite mission. For a level 2 satellite product, it is desirable to reduce the amount of required ancillary information.

Algorithms for SWE retrieval such as Rott et al. 2010 [3], Shi, 2006 [5], Cui et al. 2016 [24], and Xiong et al. 2014 [25], 2016 [26] have used a cost function-based approach. The algorithms in our previous two papers (Zhu et al., 2018 [1], 2021 [2]) also adopt the cost function approach. A reason for using the cost function approach is that the Φ , usually has more parameters than the radar observations meaning that q is larger than n . Because of this, a constraint in terms of some prior information is input. There are several issues associated with the cost function approach.

- (1) These parameters q include grain size, SWE, densities etc. The prior estimates associated with these parameters are difficult to obtain. Furthermore, the error covariance matrices are difficult to estimate. In particular, the prior estimate of grain size or scattering albedo and the associated error estimates have been difficult and have a significant number of uncertainties and historical debates
- (2) There is uncertainty in putting the relative weights w_1 for the first term and w_2 for the second term.

- (3) The retrieved SWE based on the cost function approach depends on the prior estimates, the associated variances, and the relative weight of the second term relative to the first term.
- (4) Because of the often-large number of unknowns in x , the retrieval of SWE from the cost function approach can be slow in terms of CPU requirement.

The CoReH₂O retrieval algorithm [3] is based on a single-layer semi-empirical radiative transfer (sRT) model. A cost function is used to minimize the difference between the sRT model and four radar measurements. The cost function itself is driven by two constraints: a prior on SWE and a prior on grain size. These priors had to be determined from snow climatology or derived from numerical meteorological data at regional or global coverage. Their retrieval had a satisfactory performance if the prior grain size was within 15% of the true grain size [3]. In particular, the CoReH₂O algorithm [3] has been criticized for requiring an accurate prior grain size because prior estimates of grain size are hard to achieve on a global scale.

In the algorithm of our previous two papers [1, 2], the rough soil surface scattering was removed from the measured data, and it showed increased sensitivity of SWE to σ_0 at both X and Ku bands. Next parameterized model was developed with two observations, and two unknowns thereby alleviating the problem of having more parameters than observations. This means $q = n$. The two observations are the co-polarized backscatter σ^X and σ^{Ku} . The two unknowns are SWE and the scattering albedo at X band, ω_X . A cost function approach is still used requiring a prior on the ω_X and the associated error variance.

The disadvantages of the previous algorithms are that (i) a prior and a variance estimate on the effective albedo are required, and (ii) the effective albedo, unlike grain size, is not a measurement parameter and cannot be physically measured in ground truth measurements.

There are other methods based on machine learning and neural networks that do not require any prior as well [27]. There are two ways to train machine learning methods such as ANN. The first way is to use measurement data to train the ANN. The second is to use model results to train the ANN. That certainly can be done as done in our early work [28, 29] which can be used to compare with the model parametrization. An advantage of the current method of parametrization is that it is physically based and uses multiple scattering solutions to obtain an effective single scattering solution with an effective albedo. However, for measurement data-based training, one would need a very comprehensive dataset with varying snow properties over different locations to train these ANNs for it to have the feasibility of a global application. Currently, there is no such dataset at both the X and Ku bands. Hence, we use a physics-based model that does not require too much computation and has a reasonable performance across a variety of snow types and conditions.

The novelty of this paper is that we modified the algorithm in the previous two papers and developed two improved algorithms. Neither improved algorithm requires a prior on grain size or scattering albedo. In the first algorithm, we use algebraic inversion, and the cost function is not used. In the second algorithm, a cost function is used with the prior only on SWE

and not on the albedo. The prior SWE is based on the measured time series data and not based on any models. Thus, both new algorithms avoid the historical need for prior grain size or albedo (i.e., microstructure) information. We use the parameterized bi-continuous dense media radiative transfer (DMRT) model. The parameterized model gives the X and Ku band co-polarization backscatter in terms of two parameters SWE and scattering albedo at X band (ω_X). We take an algebraic inverse of the parameterized Bic-DMRT giving the SWE and ω_X in terms of the σ^X and σ^{Ku} . This is performed numerically for a range of σ^X and σ^{Ku} values which give us a look-up table of inverses: the inverse parameterized bi-continuous DMRT look up table or I-P-Bicon/DMRT LUT.

The concept of parametrization is not new, Cui et al. 2016 [24] proposed a parameterized model to reduce the number of parameters to scattering albedo and optical thickness at the X band. Zhu et al. [1, 2] improved the parametrization by changing the parameters to scattering albedo and SWE at the X band and we employ a similar method of parametrization. The parametrization in this paper is based on a single-layer snowpack. A parametrization based on a multi-layered snowpack will result in a more complicated parameterized as different layers will have different snow bulk and microstructure properties. Du et al. 2010 [30] showed that the comparison between the backscatter for a two-layer snowpack and a single-layer snowpack with equivalent microstructure properties (such as grain size radius of the two layers scaled to find an equivalent grain size for a single-layer snowpack) The error between the two-layer model and the single layer model with the equivalent parameters is less than 0.25 dB. This means one can use equivalent microstructure properties corresponding to two or more layered snowpack and make the multi-layered snowpack into a single-layer snowpack and the result should be identical. Future studies should include the presence of ice crusts to study the effects of refrozen snow that has a sharp contrast with dry snow.

By directly inverting the two sets of equations, $\sigma^X(SWE, \omega_X)$ and $\sigma^{Ku}(SWE, \omega_X)$, we show that there are at most two pairs of solutions which usually have solutions of the SWE that are far apart. We show that it is relatively easy to pick the appropriate choice of the correct solutions using some coarse prior on SWE. This first algorithm is labeled an algebraic algorithm as it does not require a cost function. In validating the proposed algebraic algorithm for airborne data, we use a prior SWE which is intentionally 75% different from the true SWE and still achieves good performance of SWE retrieval. There is no prior imposed on the grain size or albedo. This prior SWE of 75% different from the true SWE will be straightforward to achieve in the future using hydrology models. We also show that for time series data, the retrieved SWE of the previous day itself can be used as a coarse prior for the current day retrieval. After the launch of the proposed satellite missions, time series is the rule.

The retrieval results have a root mean square error of around 25 mm of SWE for two years of the NoSREx tower data and 33 mm for the last year of the tower data. The airborne data include the SnowSAR 2013 campaign at Trail Valley Creek,

Canada, the SnowSAR 2011 and 2012 campaigns at the Arctic Research Center, Finland, and the SnowSAR 2017 campaign at the Grand Mesa, Colorado, USA. The RMSE error for the airborne data is around 37 mm of SWE for the SWE range less than 300 mm and is around 68 mm of SWE for SWE larger than 450 mm. The algorithm is fast because of the inverse parameterized Bic-DMRT look up tables.

The second algorithm uses a cost function approach but with the prior on SWE and there is no prior on the albedo. Using a time series approach, the prior SWE used is the previous day's retrieved SWE from a time series-based retrieval. The NoSREx tower data was used to evaluate this algorithm as well and performance on SWE retrieval is good with a root mean square error of 17 mm.

This paper focuses on data collected from locations that had dry snowpack conditions with open field regions without any vegetation. Vegetation can indeed significantly influence the SAR-SWE relationship. That is why SnowEx 2017 was specifically designed to collect radar and SWE data over a gradient of forest (and other vegetation) conditions. For our global SWE retrieval problem, we assume this background scattering signal measured before the arrival of snow characterizes the scattering of the above-snow forest canopy plus the below-snow ground plus low vegetation. Therefore, the satellite's own radar can measure this background signature for each pixel before snow accumulates, and it can be accounted for by the SWE retrieval algorithm.

The organization of the paper is as follows: Section 2 briefly discusses the methods of subtracting the soil rough surface component of the observed radar backscatter to get the observed volume backscatter. Section 3 will discuss the parameterized bi-continuous DMRT model used for the retrieval. This model is derived from regression training done on the full bi-continuous DMRT model. Section 4 will describe the solution space of the parameterized bi-continuous DMRT model, where we will show that there are up to two solutions at most for the problem and what the separation in the solution looks like. We will also show the generation of the I-P-Bicon/DMRT LUT. Section 5 will contain the four airborne datasets and the retrieval performance on the airborne data where we use prior SWE as 75% different from the true SWE. Next, the tower time series data are discussed, and retrieval is based on time series. Section 6 describes the cost function algorithm, the cost function with prior on SWE only. We also illustrate the effects of the prior weighting factor and the error covariance in the cost function. Section 7 gives a summary of the algorithms and the retrieval accuracies.

2. SUBTRACTION OF ROUGH SURFACE SCATTERING CONTRIBUTIONS

In addition to volume scattering, there are contributions to radar backscattering from the rough surface between the snow and the soil below. To retrieve the SWE, the rough surface scattering contributions are subtracted in our previous two papers [1, 2] and this paper uses same method. In the review paper [4], various methods of such subtractions are described which include using L band observations over snow cover (as L band pen-

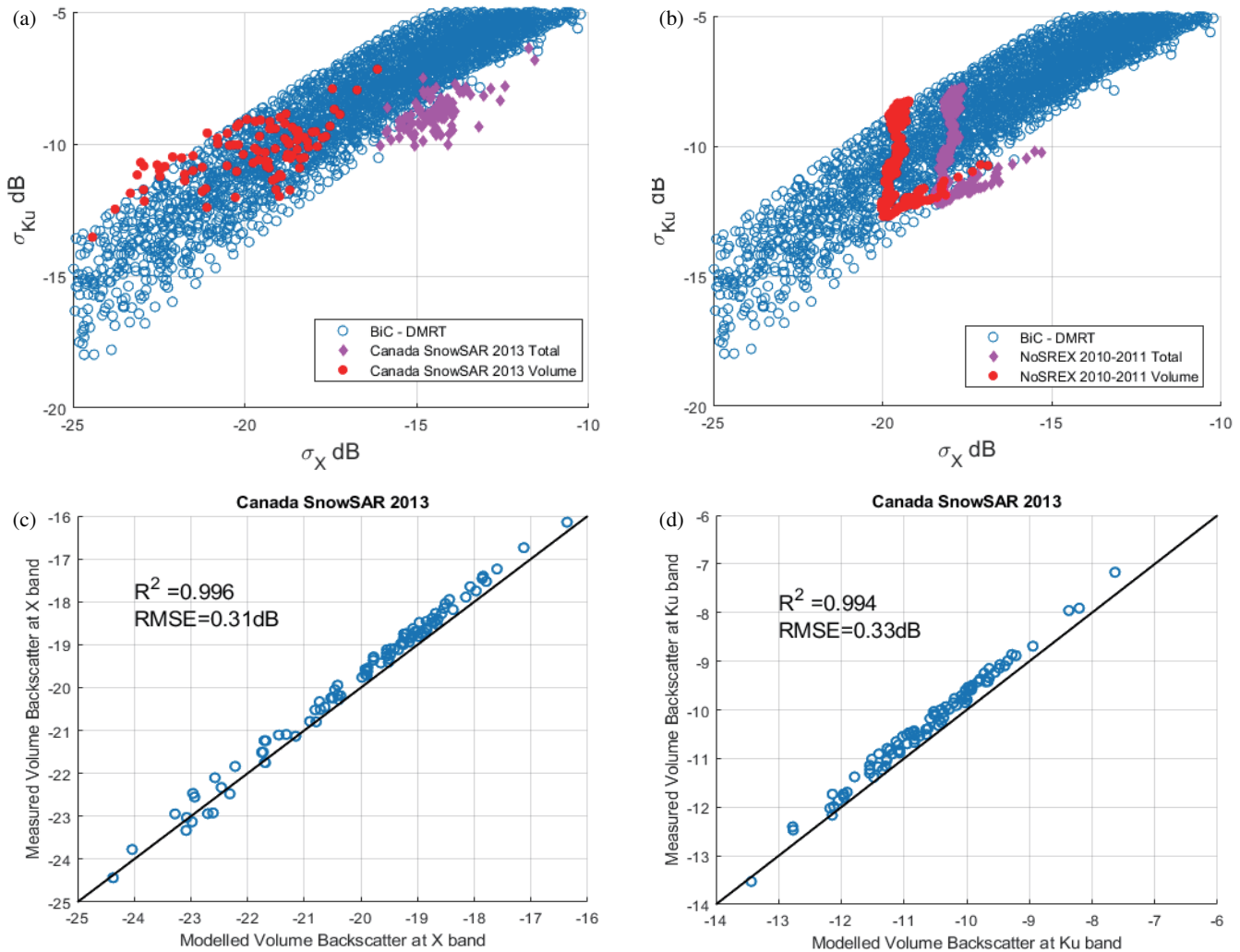


FIGURE 1. SnowSAR 2013 airborne measurements (a) and NoSREx 2010–2011 tower measurements (b) compared to Bic-DMRT model. Modelled volume backscatter compared to measured volume backscatter at X band (c) and Ku band (d) for SnowSAR 2013 campaign.

etrates through snow and only sees the rough surface below the snow) to estimate the soil moisture and rms height of the surface. The measurements used in subtraction include radar observations before the snow season, backscattering measurements at the L Band that will be available from NISAR, and backscattering measurements from Sentinel 1 at the C band. Theoretical models of rough surfaces are from Oh et al. [31] in the past. However, Oh's empirical algorithm is only based on measurements of 4 rough soil surfaces. Recently full wave simulations of rough soil surface scattering have been performed from the L band to the Ku band [32]. Look-up tables will be used in the future for the subtraction of rough surface scattering. As shown in Figure 1, the subtraction of rough surface scattering brings the measured data to overlap with the volume scattering model of bi-continuous DMRT. With the advance of rough surface scattering models from the L band to the Ku band [32], and the availability of SMAP, NISAR, and Sentinel 1 data, the removal of rough surface effects can be based on models and satellite data rather than ancillary information.

3. PARAMETERIZED BI-CONTINUOUS DMRT MODEL

As discussed in the Introduction, when the number of unknowns q exceeds the number of observations n , there are generally an infinite number of solutions. In such a case, the SWE retrieval algorithm requires constraint on the q number of unknowns with prior estimates of parameters and error variances. To have a finite set of solutions we need to have a model which has the same number of observations and unknowns, that is $q = n$. In the case of two observations of dual frequency copolarized X and Ku bands the model must be parameterized in terms of two unknowns. In our work, the two unknowns are SWE and the effective X band scattering albedo ω_X . Look-up tables of bi-continuous DMRT are generated that are based on a range of parameters of SWE, equivalent grain size, and equivalent correlation lengths, snow densities, etc.. Through regression analysis, the DMRT model results are parameterized to two unknowns, which are SWE and ω_X .

In the Bic-DMRT model, first many realizations of bi-continuous media of air and ice are generated which represents

TABLE 1. Parameters of Bic-DMRT for LUT generation.

Parameters	Minimum	Maximum
Snow density, ρ (kg/m ³)	40	450
Snow Depth (m)	0.1	2
b	0.6	2
$\langle\zeta\rangle$ (m ⁻¹)	5000	17000

computer-generated snowpack [17,33]. Volume integral equation which is solved by discrete dipole approximation (DDA) is used to find the full wave solution of each of the realization of bi-continuous media and find the phase matrix of the snowpack [33]. Once the phase matrix is found, the DMRT equation is solved to find the backscattering from the computer-generated snowpack [16,17]. For a single layer of snowpack, there are four inputs to the Bic-DMRT model, which are snow depth d , density ρ , snow microstructure parameters $\langle\zeta\rangle$ and b . The mean wavenumber $\langle\zeta\rangle$ with unit of m⁻¹ is proportional to the SSA of the snow. The dimensionless parameter b describes the aggregation of snow particles with a smaller b corresponding to larger aggregates of ice grains. Thus $\langle\zeta\rangle$ and b represent equivalent grain sizes, correlation lengths and aggregations. Analytical closed-form expressions of the bi-continuous media were also derived [33] so that the bi-continuous media model can be made to correspond to the random media model [34,35].

Outputs of Bic-DMRT are volume scattering at X and Ku bands (σ^X and σ^{Ku}), scattering albedo at X and Ku band (ω_X and ω_{Ku}), optical depth at X and Ku band (τ_X and τ_{Ku}), and absorption loss. Figure 1 shows the backscatter outputs of the Bic-DMRT model along with volume scattering radar observations for the SnowSAR 2013 airborne campaign and the NoSREx 2010–2011 tower campaign at VV polarization. Figures 1(a) and 1(b) show the effects of rough surface scattering and that removing the rough surface scattering component brings the measured data into the regime of the bi-continuous DMRT model. Figures 1(c) and 1(d) show the direct comparison of the measured volume scattering and the modeled volume scattering at the X and Ku bands, respectively, for the Canada SnowSAR 2013 campaign. Both Figures 1(c) and 1(d) show good agreement with the bi-continuous DMRT model with root mean square error less than 0.5 dB.

The bi-continuous DMRT model has a lower and more varying frequency dependence (around 2.7th to 4th power of frequency) on scattering compared to HUT, MEMLS and the DMRT/QCA. This is because, in addition to the grain size parameter $\langle\zeta\rangle$, there is the aggregation parameter b in the bi-continuous media. It can be seen in Figure 1(a), where for a fixed modeled σ_X , the modeled σ_{Ku} is about 6 dB to 10 dB higher, which corresponds to 2.7th and 4th power of frequency respectively. Both the HUT and MEMLS are empirical models. They use a fixed frequency dependence around 2.7th power of frequency [36,37]. These dependencies were derived by fitting ground-based snow measurements to observations. This fixed frequency dependence does not encompass all the physics

due to aggregation and grain size. The DMRT/QCA has a higher frequency dependence of 3.3rd power to 4th power of frequency [14]. It is because DMRT/QCA assumes that the ice particles in a snowpack are spherical in shape and are sticking together which is controlled by the stickiness parameter. This results in a much smaller difference between the modeled σ_X and the modeled σ_{Ku} when compared to the bi-continuous DMRT. Since the parametrization of the bi-continuous DMRT is based on the model parameters only the lower frequency dependence of bi-continuous DMRT is carried over to the parameterized model as well and will give better performance in SWE retrieval at X and Ku bands compared to these other models. The model is next parameterized to two parameters so that $q = n = 2$. A look-up table (LUT) of the output of Bic-DMRT is generated for varying depth, density, $\langle\zeta\rangle$ and b for both X and Ku bands. Table 1 shows the parameters used in the LUT generation.

Regression training is then performed between ω_X vs ω_{Ku} , τ_X vs τ_{Ku} , first order scattering at X band vs multiple scattering at X band and first-order scattering at Ku band vs multiple scattering at Ku band respectively. The goal of these curve fitting between the outputs of the LUT is to reduce the number of parameters in predicting the volume scattering from a singlelayer snowpack to two. Combining these regression relations from the Bic-DMRT LUT gives the parameterized Bic-DMRT model. Equations (1) and (2) give the co-polarized parameterized backscattered volume scattering at X and Ku band in terms of two parameters: SWE and scattering albedo at X band, ω_X respectively. Cross-polarization can also give important information on snow properties. The contribution of cross-polarization arises from 2 factors one, the aggregated ice grains that result in irregular shapes and second, the double volume scattering which is diffuse scattering. As shown in a previous paper, the cross-polarization results of bi-continuous DMRT are in good agreement with the NoSREx data [17]. However, there is not enough airborne data to validate the parametrization and the retrieval algorithm. Hence, this paper (and the retrieval algorithm) only uses co-polarization. Cross-polarization will be studied in the future when more accurate airborne cross-polarization data are available.

$$\sigma_{VV}^X (dB) = -2.81 + 0.96 \times 10 \log \left\{ 0.75 \cos \theta_t \omega_X \left[1 - \exp \left(-\frac{2SWE}{9745 (1 - \omega^X) \cos \theta_t} \right) \right] \right\} \quad (1)$$

$$\sigma_{VV}^{Ku} (dB) = 0.054 + 1.12 \times 10 \log$$

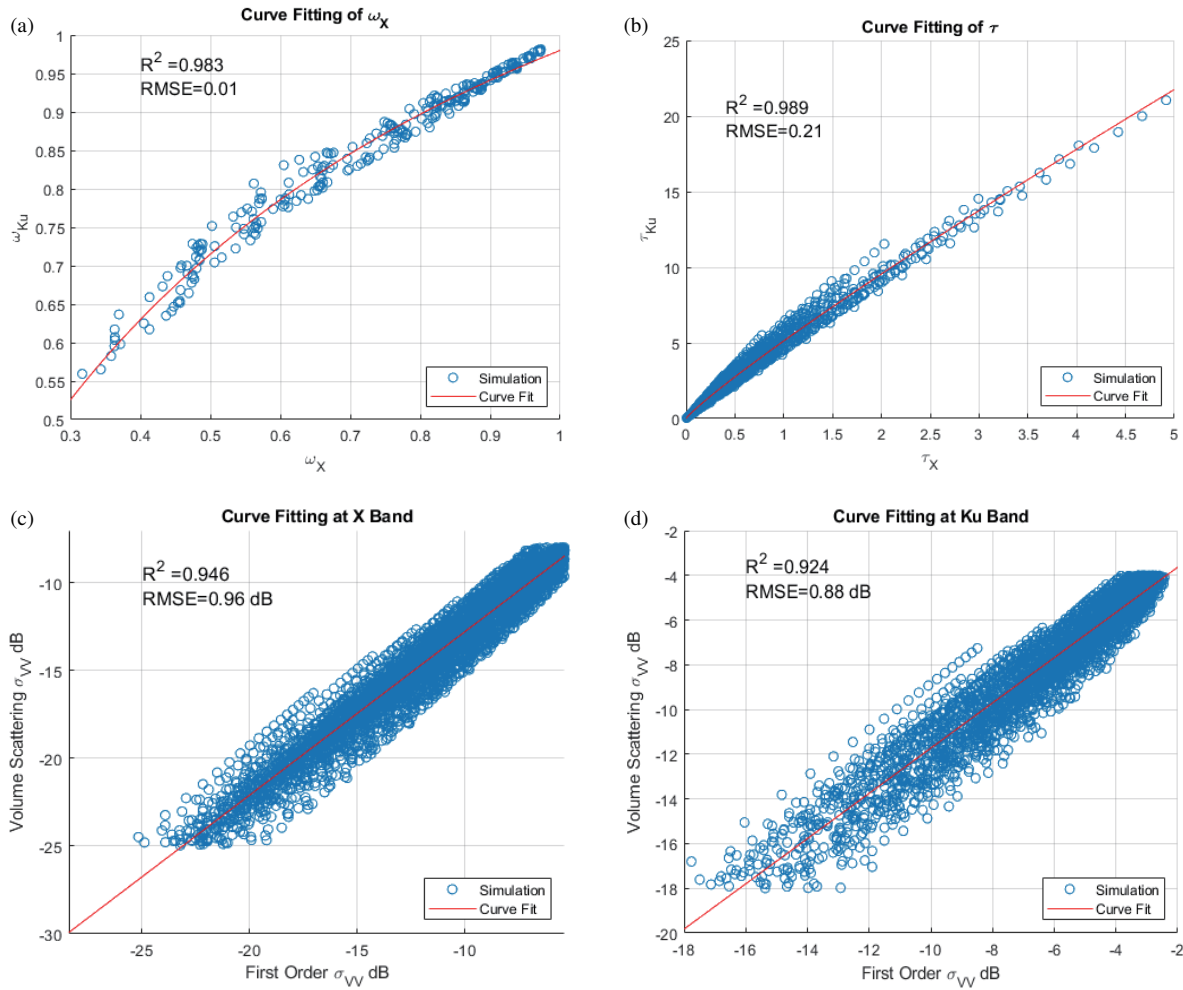


FIGURE 2. Regression fit between the outputs of Bic-DMRT LUT.

$$\left\{ \begin{array}{l} 0.75 \cos \theta_t \left(\frac{\omega_X}{0.656\omega_X + 0.369} \right) \\ \times \left[1 - \exp \left(-\frac{2}{\cos \theta_t} \left(5.37 \left(\frac{SWE}{9745(1-\omega_X)} \right)^{0.972} \right) \right) \right] \end{array} \right\} \quad (2)$$

These two Equations (1) and (2) were reported in the Zhu et al. 2018 [1] and have been generated for SWE range from 50 mm up to 350 mm. Even though a SWE of up to 350 mm is sufficient for a lot of cases, there are places globally that have SWE exceeding 350 mm. We next extend the regression models to have ranges of SWE from 50 mm to 850 mm. To extend the range, we follow a similar procedure as in [1, 2].

Figures 2(a) to (d) shows the curve fits for ω_X vs ω_{Ku} , τ_X vs τ_{Ku} first order scattering at X band vs multiple scattering at X band and first-order scattering at Ku band vs multiple scattering at Ku band respectively for the extended SWE range.

Figures 2(a) and (b) show the nonlinear fit between ω_X vs ω_{Ku} , τ_X vs τ_{Ku} respectively. These relations are

$$\omega_{Ku} = \frac{\omega_X}{0.6421\omega_X + 0.3782} \quad (3)$$

$$\tau_{Ku} = 5.131 (\tau_X)^{0.8977} \quad (4)$$

Figures 2(c) and (d) show the linear fit between equivalent first order scattering at the X band vs multiple scattering at the X

band and equivalent first order scattering at the Ku band vs multiple scattering at the Ku band respectively which are given by

$$\sigma_{VV}^X = -2.496 + 1.001 \times \sigma_{VV}^{X,1st} \text{ (dB)} \quad (5)$$

$$\sigma_{VV}^{Ku} = -0.4401 + 1.139 \times \sigma_{VV}^{Ku,1st} \text{ (dB)} \quad (6)$$

where the equivalent first order scattering is given by,

$$\sigma_{VV}^{q,1st} = 0.75 \cos \theta_t \omega_q \left[1 - \exp \left(-\frac{2\tau^q}{\cos \theta_t} \right) \right], \quad q = X \text{ or } Ku \quad (7)$$

Using these regression relations and the equivalent first order scattering formulation, we obtain a set of parameterized Bic-DMRT equations below to extend the range of SWE from 50 to 850 mm.

$$\sigma_{VV}^X \text{ (dB)} = -2.496 + 1.001 \times 10 \log \left\{ 0.75 \cos \theta_t \omega_X \left[1 - \exp \left(-\frac{2(SWE - 45.25)}{6404(1 - \omega_X) \cos \theta_t} \right) \right] \right\} \quad (8)$$

$$\sigma_{VV}^{Ku} \text{ (dB)} = -0.4401 + 1.139 \times 10 \log$$

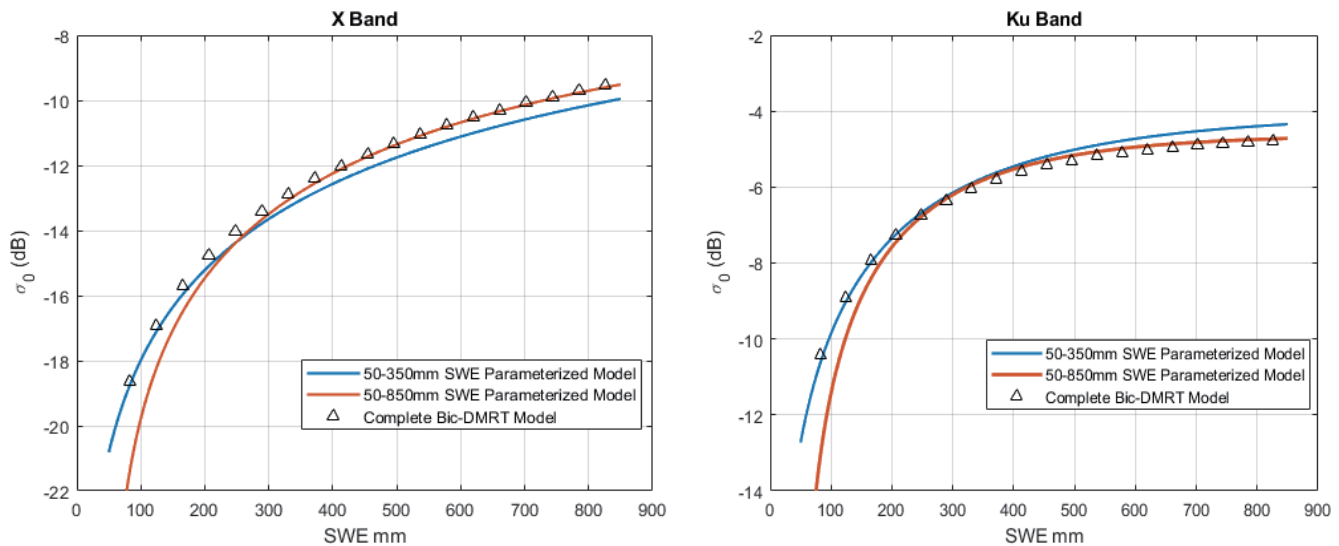


FIGURE 3. Comparison of the of the parameterized model for the two ranges of SWE with the full BiC/DMRT model.

$$\left\{ \begin{array}{l} 0.75 \cos \theta_t \left(\frac{\omega_X}{0.6421\omega_X + 0.3782} \right) \\ \times \left[1 - \exp \left(-\frac{2}{\cos \theta_t} \left(5.131 \times \left(\frac{SWE - 45.25}{6404(1 - \omega_X)} \right)^{0.8977} \right) \right) \right] \end{array} \right\} \quad (9)$$

Figure 3 compares the parameterized model based on Equations (1) and (2) and Equations (8) and (9). We plot the backscatter σ_0 with respect to SWE at a fixed $\omega_X = 0.6$. The plots show three comparisons, the blue and red curves correspond to the 50–350 mm range parameterized model (1 and 2) and to the 50–850 mm range parameterized model (8 and 9) respectively. The black triangles are from the full bi-continuous DMRT model (without parametrization). We can see that for lower ranges of SWE from 50 till 200 mm, 1 and 2 match the complete model whereas for higher values of SWE from 400 to 850 mm, 8 and 9 match the complete model better. That means, we cannot use 8 and 9 for the full range of SWE even though it was designed for 50–850 mm. Between 200 and 400 mm, both the parameterized model gives a very close match to the full model. But it is the before and after this middle 200–400 mm range that we must use the model that was specifically designed for that range. Hence, when dealing with the SWE range of less than 350 mm we use 1 and 2 and for SWE beyond 350 mm till 850 mm, we use 8 and 9. For the time series-based retrieval discussed in section 5.2, we always start with 1 and 2 and when we reach a retrieve SWE of close to 350 mm, we switch to 8 and 9. The buffer zone of 200–400 mm of SWE, where both sets of equations give the same (or very close) results, makes the transition from one set of equations to another possible without many errors. The Equations (8) and (9) were parameterized on 50 to 850 mm of SWE and not on 350 to 850 mm (which is the range it is being used for) because the curve fits in Figure 2 results in a better correlation and lower RMS error if 50 to 850 mm of SWE is used instead of 350 to 850 mm.

The parameterized model was not extended beyond 850 mm of SWE as there are no X and Ku band radar datasets available that include such high values of SWE making validation not possible. In this paper we use two sets of parameterizations

for the two SWE ranges of 50 to 350 mm and 350 to 850 mm. In the future, after the satellite is launched, there will likely be several sets of parameterizations that vary with the ranges of SWE and the characterizations of microstructures of snow. The parameterized equations will continue to be studied, improved, and adapted to regions globally. Since there are two equations and two unknowns, there is only a finite set of solutions. We next algebraically invert the two equations to obtain the inverse relations of SWE and ω_X in terms of σ^X and σ^{Ku} .

4. ALGEBRAIC ALGORITHM WITHOUT COST FUNCTION

4.1. Solution Space of Parameterized Bi-Continuous DMRT Model

The set of parameterized Bic-DMRT equations in either Equations (1) and (2) or Equations (8) and (9) are two equations, σ_{VV}^X and σ_{VV}^{Ku} in terms of two unknown parameters SWE and ω_X . From the measured volume scattering from an airborne or tower measurement, one can solve for SWE and ω_X . We found that Equations (1) and (2) and Equations (8) and (9) have two pair of solutions at most. The two SWE solutions are also far apart, which means only a coarse prior of SWE is sufficient to pick the correct solution. We illustrate these solutions by using the σ^{Ku} and σ^X plot and the effective ω_X vs SWE plot.

Figure 4 shows the different solution types for the parameterized Bic-DMRT equations. The different color region corresponds to the different type of solution that one can get from the two equations. This solution space is generated for the SWE range of 50 to 350 mm and ω_X from 0.15 to 0.8. The black region is the region of volume backscattering at X and Ku bands that will not result in any solution. This region corresponds to the case when σ_{VV}^X is larger than σ_{VV}^{Ku} , which is physically not possible or σ_{VV}^X and σ_{VV}^{Ku} are outside the range of the Bic-DMRT model. The red region is the region where there is one solution of SWE for a given σ_{VV}^X and σ_{VV}^{Ku} . The

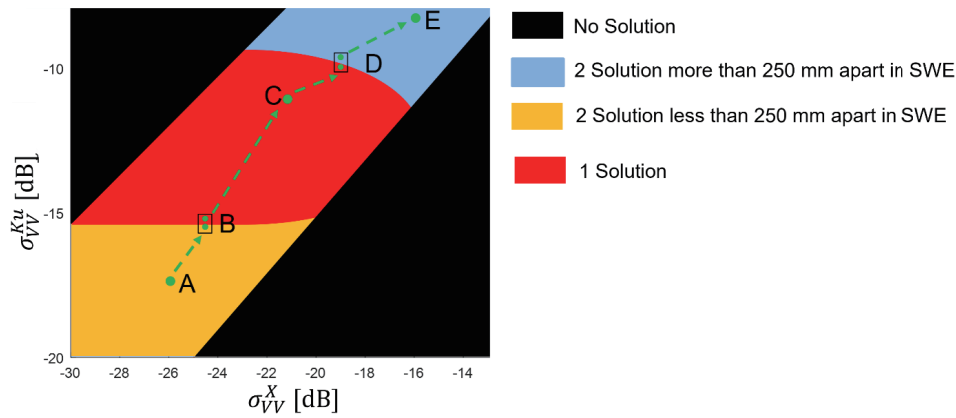


FIGURE 4. Solution space of the parameterized Bic-DMRT model. Different regions correspond to different types of 16 solutions.

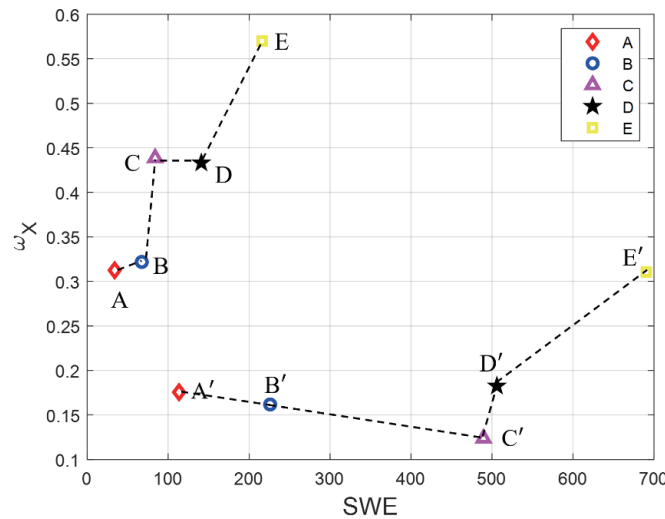


FIGURE 5. Two solutions for the set of σ_{VV}^X and σ_{VV}^{Ku} values at each marker A, B, C, D, and E.

yellow and blue regions are where we have two solutions that are less than 250 mm apart and more than 250 mm apart. The limit of 250 mm of SWE is taken so that the correct solution of SWE is easier to pick with the help of a coarse prior on SWE. The coarse prior is just to assist in choosing the correct solution out of the pair of solutions. There is no need for an error estimate of the prior. This prior can be the previous day’s retrieved SWE in case of time series data. For the case of airborne data, we validate the algorithm by selecting a prior SWE that is 75% different from that of true SWE for airborne data. This choice is just a test of the algorithm because, in actual implementation, the true SWE is not known. In the airborne data of this paper, the true SWE was provided by ground measurements. In actual implementation, we only need a coarse prior from some hydrology model in the future or from time series data in the future. As a result of this, a prior on grain size or ω_X that are in our previous two papers [1, 2] is completely avoided. Priors and error estimates on these snow microstructure parameters are more difficult to evaluate than a coarse prior on SWE.

The different regions in Figure 4 are marked with A, B, C, D and E. These markers also show the evolution of σ_{VV}^X and σ_{VV}^{Ku} with the increase in SWE, representing the seasonal behavior

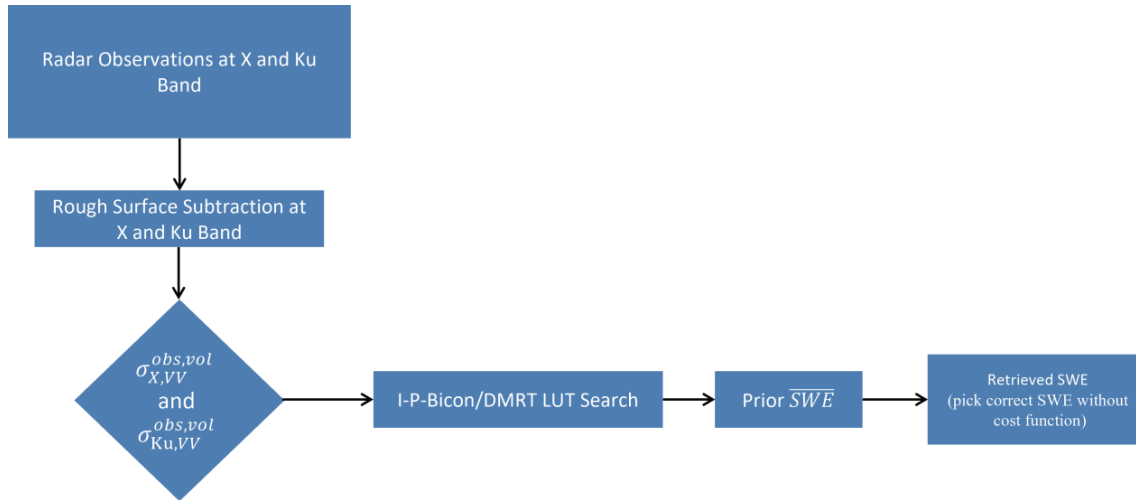
of snow from the start of the season up until just before the onset of snow melt. Each σ_{VV}^X and σ_{VV}^{Ku} corresponding to the marker will have two solutions of SWE as shown in Figure 5, one unprimed answer and the other primed answer. The two solutions of SWE for each σ_{VV}^X and σ_{VV}^{Ku} will start with less than 250 mm between them and as the season goes on, they will move further apart. This is illustrated in Figure 5 as well as A and A’ start with less than 250 mm apart, and by the time we reach E and E’, the separation is much more than 250 mm. This is the basis for the time series-based retrieval, where, as we go into the season, it becomes easy to pick the correct branch. In Figure 5, C has two solutions, but one solution has ω_X less than 0.15, which is why C is in the red region for Figure 4 (Figure 4 was made with ω_X greater than 0.15). The details for the time series algorithm are in Subsection 5.2.

4.2. Inverse Parameterized Bi-continuous DMRT Look up Table (I-P-Bicon/DMRT LUT)

The solution space of the parameterized bi-continuous DMRT equations show that there are two sets of solution for SWE and ω_X . To have a fast retrieval algorithm, we generate an inverse

TABLE 2. Ranges of σ_{VV}^X and σ_{VV}^{Ku} for LUT generation.

	SWE 50 to 350 mm		SWE 50 to 850 mm		Interval
	Minimum	Maximum	Minimum	Maximum	
σ_{VV}^X	-30	-12	-30	-6	0.01
σ_{VV}^{Ku}	-20	-5	-20	-3	0.01

**FIGURE 6.** Flowchart of the inversion-based algorithm using I-P-Bicon/DMRT LUT.

look up table to express two sets of solutions of SWE and ω_X in terms of the measured volume scattering at X and Ku band, σ^X and σ^{Ku} . We shall label this as an inverse parameterized Bi-continuous DMRT look up table or I-P-Bicon/DMRT LUT. We use a prior on SWE to pick the correct solution between the two. Since there are two sets of parameterized DMRT equations, we must generate two look-up tables. One for Equations (1) and (2) corresponding to the SWE range of 50 to 350 mm and the second table for Equations (8) and (9) corresponding to the SWE range of 50 to 850 mm. Table 2 shows the values used for σ_{VV}^X and σ_{VV}^{Ku} in the LUT generation for the two ranges of SWE.

We get the measured volume backscatter from the radar and compare the backscatter value to the value of backscatter the in a made LUT. Once we have the backscatter value in the LUT, we can directly pick the correct SWE by using a prior SWE. In this way, the need to search for the answer in a big solution space is eliminated. The algebraic algorithm is expressed in the flowchart in Figure 6.

5. RESULTS OF RETRIEVAL OF SWE USING THE ALGEBRAIC ALGORITHM

In this section, we map the algebraic algorithm using both airborne and tower-based radar datasets. These datasets span different geo-locations, different types of snow, and different amounts of snow.

5.1. Airborne Data

In this paper, four sets of airborne data are studied which were all part of different SnowSAR campaigns: Finland SnowSAR 2011 [38], Finland SnowSAR 2012 [38], TVC SnowSAR 2013 [38], and Grand Mesa SnowSAR 2017. The first three SnowSAR campaigns were part of the European Space Agency's airborne SAR missions between 2010 and 2013. The Grand Mesa SnowSAR 2017 was part of NASA's 2017 SnowEx campaign. The data acquisition for the Finland campaigns happened in two separate winters of 2010–2011 and 2011 to 2012 respectively in Sodankyla and Saariselka. These sites represent a boreal/taiga type of environment. The flights using the SnowSAR instrument happened on March 17, 2011, and data from four flight tracks were collected at both X-band (9.6 GHz) and Ku-band (17.2 GHz), represented as Finland SnowSAR 2011. More extensive data were acquired between December 19, 2011, and March 24, 2012, with a total of ten flight missions, represented as Finland SnowSAR 2012. The SWE recorded for both winter campaigns was from 70 mm to 150 mm.

TVC SnowSAR 2013 campaign happened in the winter of 2012–2013 in the tundra region of Trail Valley Creek in Canada. Two sets of SnowSAR flights were performed at TVC, one on March 13 and 14 2013, and the other on April 8 and 9 2013, both collected data at X-band (9.6 GHz) and Ku-band (17.2 GHz). Although the number of flights was limited, extensive in-situ measurements of SWE and snow bulk and microstructure properties were taken as part of the campaign. SWE recorded for

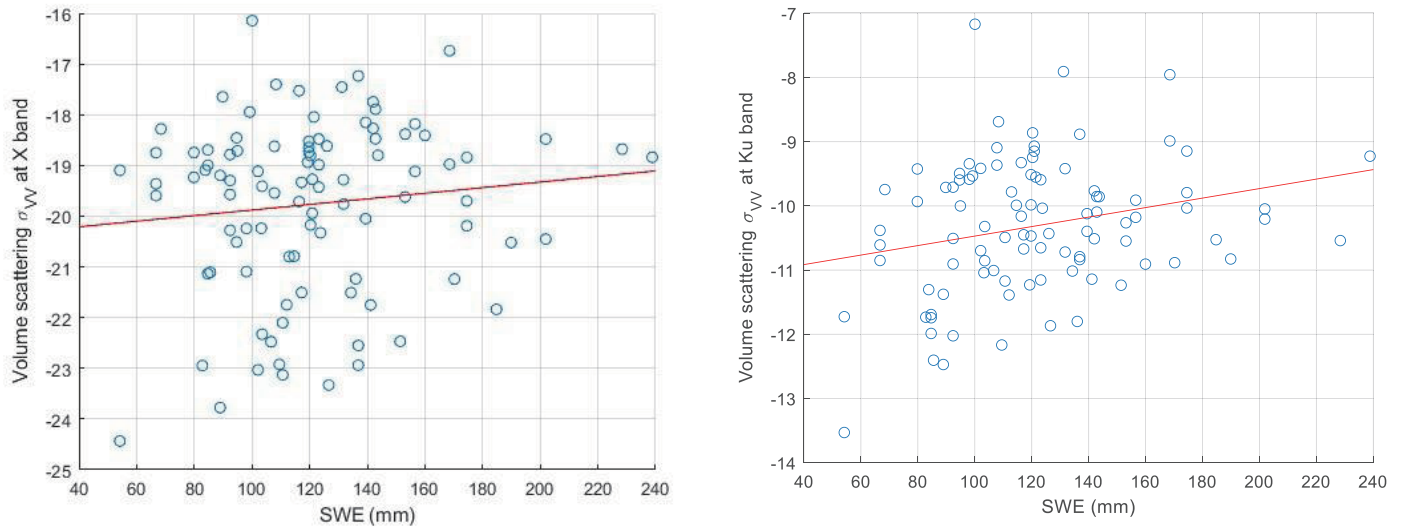


FIGURE 7. Measured volume backscatter verses SWE at X and Ku band for TVC SnowSAR 2013 data.

this location was from 50 mm to 250 mm. For this paper, only the flights in the month of March are used for validating the retrieval as the snow during March was dry.

As a part of the SnowEx 2017 campaign, the SnowSAR synthetic aperture radar was used to collect backscatter amplitude images at X (9.6 GHz) and Ku (17.2 GHz). The SnowSAR instrument flew between 16 February 2017 and 22 February 2017 and captured images across Grand Mesa where the ground campaign took place. For the retrieval analysis, however, we only use the data collected on 21 February 2017 as that day had the highest coverage by the instrument. Grand Mesa had the highest snowfall of all the data studied in this paper with SWE ranging from 450 mm to 750 mm.

All these campaigns were accompanied by field measurements as well where in-situ measurements of SWE and transect of depth and density measurements were also taken. However, not all the ground data were co-located with the flight path of the airborne SAR instrument. Hence, for the validation of the retrieval algorithm, only the in-situ snow pits co-located with the SnowSAR observations are used. The SWE from these co-located in-situ snow pits is considered as “true SWE” and is compared against the retrieved SWE. Because of this, the number of data points used in the retrieval varies significantly depending on the dataset and how many in-situ measurements were taken. The TVC SnowSAR 2013 has 103 data points of true SWE, Finland SnowSAR has 5 and 21 for the 2011 and 2012 campaigns respectively and the Grand Mesa SnowSAR 2017 has 11 data points of true SWE. Figure 7 shows the SWE plotted against volume scattering of measured σ_{VV}^X and σ_{VV}^{Ku} for the TVC SnowSAR 2013 data. The reason that the data of Figure 7 shows a weak correlation between the measured volume backscatter and the SWE is that the radar backscatter depends both on SWE and ω_X . Which means that two snowpacks with different amounts of SWE can have the same backscattered σ_0 if the ω_X is adjusted appropriately. The data presented in Figure 7 was collected over different locations in the Trail

Valley Creek region for just two days. Because of this, there is only special variability and no temporal variability in the data. This can result in one snowpack at one location with low SWE but a higher ω_X and another snowpack at some different location with a higher SWE but a low ω_X . Both locations will have a near similar level of backscatter.

For the Finland and the TVC SnowSAR data, since the total recorded SWE was less than 350 mm, we use Equations (1) and (2) of the parameterized DMRT model. We find the σ_{VV}^X and σ_{VV}^{Ku} in the I-P-Bicon/DMRT LUT which corresponds to the observed volume scattering and get the two sets SWE and ω_X solution for each pair of σ_{VV}^X and σ_{VV}^{Ku} from the LUT. Figure 8 shows the two solutions for the TVC SnowSAR dataset.

To find the correct solution, we use a prior on SWE. Since in this case we know the true SWE, in order to validate the algorithm, we deliberately choose a prior SWE that is “quite wrong”. The “quite wrong” prior selected is 75% different from the true SWE, which is a large difference from the true SWE. We show that the algorithm still works with this “quite wrong SWE” large difference from the true SWE.

What this shows that in the actual implementation, we only need a prior that is 75% within the true prior which is unknown. In actual implementation, the observed volume scattering at X and Ku band is used to find the two solutions of SWE from the I-P-Bicon/DMRT LUT. This is shown in red and blue dots in Figure 8 for the case of TVC SnowSAR data. The correct SWE is picked by using a prior on SWE, which in this case is 75% different from true SWE. To find these solutions, there is no constraint on parameter nor cost function. This method fully relies on the model and does not put any weight on any hydrological or climatological model. The Equations (1) and 2 are being solved exactly to get the LUT and find the solution of SWE. Only a coarse prior on SWE of 75% different from true SWE is used to find the correct answer. The SWE retrieval result is shown in Figures 9(a), (b), and (c) for TVC SnowSAR 2013 data and the two years of Finland SnowSAR data respec-

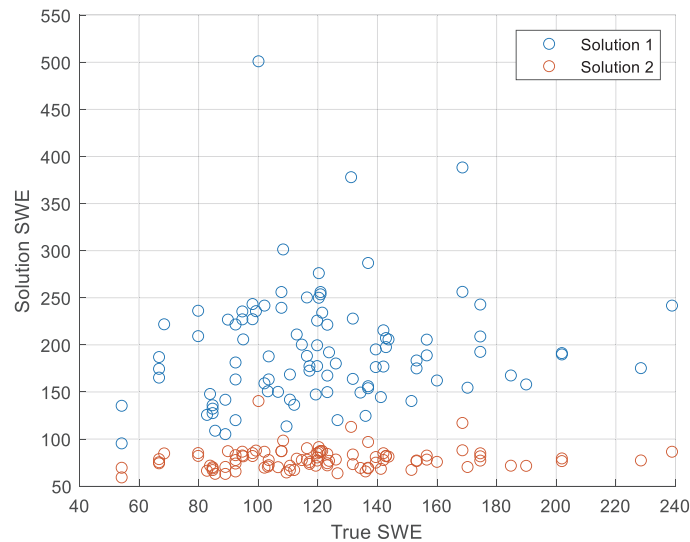


FIGURE 8. Two solutions of SWE from the parameterized DMRT solver for TVC SnowSAR 2013 data.

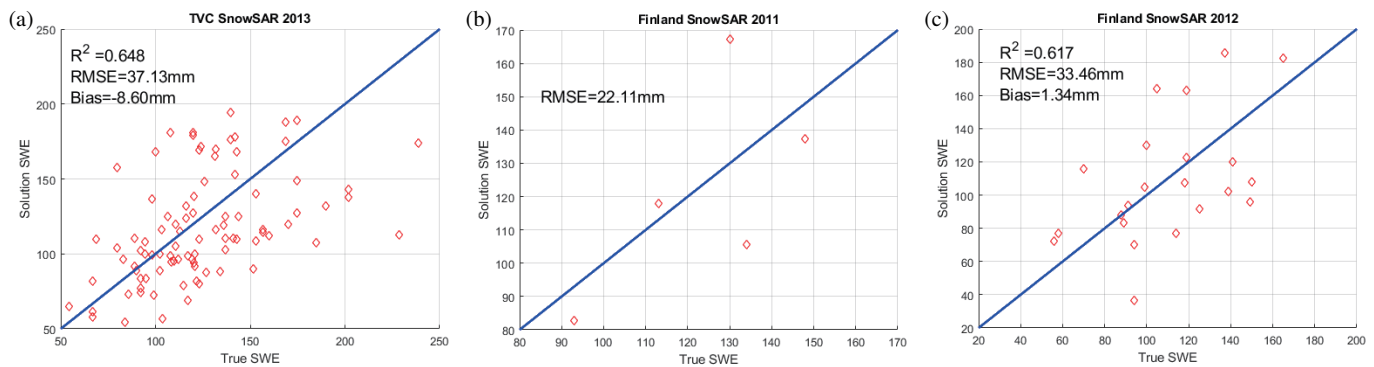


FIGURE 9. Retrieve SWE versus true SWE (in-situ measured SWE) for: (a) TVC SnowSAR 2013, (b) Finland SnowSAR 2011 and (c) Finland SnowSAR 2012.

tively. The root mean squared error for each of the campaign is less than 40 mm of SWE.

For the Grand Mesa SnowSAR 2017 data, we need to use the second I-P-Bicon/DMRT LUT, generated from Equations (8) and (9) of the parameterized DMRT model as the SWE range is from 450 mm to 750 mm. The procedure to find the correct SWE solution is the same as illustrated above with just the change in the LUT. In this case as well, we use a prior SWE of 75% different than that of true SWE as the solver's initial guess. Figure 10 shows the result for the SnowSAR 2017 data.

With a mean square error of 68 mm, the 2017 SnowSAR has the worst performance among the airborne datasets. The performance is expected at higher values of SWE as the sensitivity of the volume backscatter to SWE starts to decrease at high value of SWE. The co-polarized backscatter starts to saturate as we go higher in SWE and thus the errors increase as well.

5.2. Tower Data and Time Series Retrieval

The Finnish NoSREx data set (Lemmetyinen et al., 2016 [39]) collected by the Finnish Meteorological Institute (FMI) is used to evaluate the algorithm in the paper. The NoSREx cam-

paigns were initially performed for four successive winters 2009–2013 at the Arctic Research Center in Sodankylä, northern Finland. Both active and passive microwave instruments were installed on tower platforms. The active measurements were provided by SnowScat, a scatterometer operating at 10.2, 13.3, and 16.7 GHz (X- to Ku-band) with full polarization. In this paper, we use three years of NoSREx data, 2009–2010, 2010–2011 and 2012–2013 and only active radar measurements at 10.2 and 16.7 GHz. The data from year 3 (2011–12) was not used because of instrument malfunction and a very limited observations from dry snow season [2]. Figure 11 shows the time series of backscatter at Ku band and SWE for the year of NoSREx 2010–2011. The rest of the year has similar time series observations. Only the dry season is used for the retrieval analysis.

The time series-based retrieval takes advantage of the fact that at the start of the season, it is known that the SWE will be a small quantity. One can directly pick the correct solution between the two sets of SWE solutions for the first retrieval of the season by simply picking the smaller of the two solutions. As illustrated in Figure 5, the first retrieval of the season corresponds to solution A or A'. We pick the solution A as that

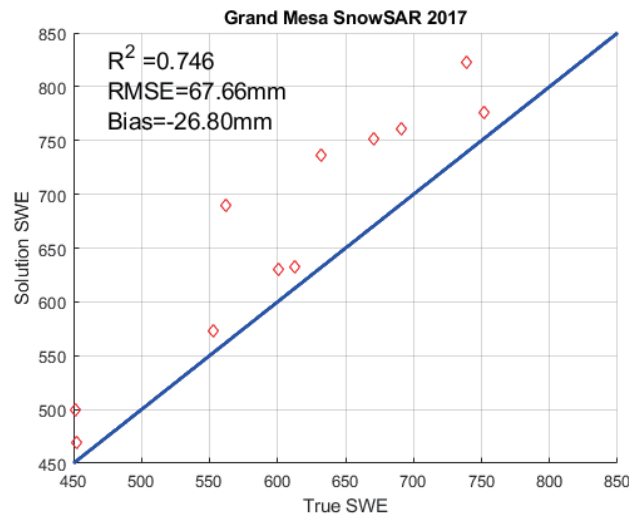


FIGURE 10. Retrieve SWE versus true SWE (in-situ measured SWE) for Grand Mesa SnowSAR 2017.

has a smaller value than A' . Then, we move to the second day and use the first day's retrieved SWE as a prior for the second day's retrieval. For the second day, from the measured volume backscatter at the X and Ku bands, we again find the two solutions of SWE. We pick the solution of SWE which is closer to the first day's retrieved SWE for the second day. Then, we solve for SWE on the third day using the retrieved SWE on the second day as a prior and the process keeps on repeating until the last day of dry snowfall. Note that the time series prior only helps us to choose the solution from the inverse parameterized DMRT. The idea behind this time-step approach is that as the season goes on, the two solutions will drift further apart as shown in Section 3, making the choice of correct solution based on the previous day's solution easier. A SWE difference of more than 250 mm between two consecutive days is an extremely unlikely scenario and the choice of correct answer based on the previous day's result will be valid.

For the NoSREx datasets, the daily step in time for both SWE and backscatter observations is used, and December 1 of each experiment year is taken to be the first day of the season (first day of retrieval). So, for NoSREx 2010–2011, first day of the season to retrieve SWE is taken to be December 1, 2010. On this day, the measured backscattered signal is $\sigma_{VV}^X = -21.90$ dB and $\sigma_{VV}^{Ku} = -12.01$ dB for volume scattering only. From I-P-Bicon/DMRT LUT, we get one solution as 71 mm of SWE and the other solution as 202 mm of SWE. Thus, we pick the smaller solution of 71 mm for the first day. Then, we use this 71 mm of SWE as a prior for the second day and pick the solution close to 71 mm for the second day and keep repeating the process. Figure 12 shows the retrieved SWE for the three years.

The winter year of 2009–2010 and 2010–2011 shows good retrieval performance with a root mean squared error of less than 25 mm of SWE for both, with 2010–2011 having an error of 19 mm. The 2012–2013 had the worst performance between the three years with an error of 33.13 mm of SWE. This can be explained due to the irregularities in the measurement as re-

ported in [39]. The backscatter at both X and Ku bands initially decreased slightly and then remained constant through the majority of the season, resulting in a worse performance compared to the other two years. Although the NoSREx data was available in a daily timestep, it is not always the case. In certain situations, a time series data may only be available at a 2- or 3-day time step. In that case, we will also need to include the 75% different from the true SWE in the prior to have accurate retrievals. The prior when the timesteps are a few days apart will be an average of the previous timestep's retrieved SWE and the 75% different of the true SWE.

We use the previous time step SWE as the prior SWE in the tower data. In the future, when the satellite missions have been launched and there are time series data every 3–4 days, the time series approach as described in this section will be used in the satellite data retrieval of SWE.

The use of LUT decreases the computation time to find the correct SWE answer as, instead of inverting for the problem, we are essentially picking the answer from a table. Table 3 shows the computation time of finding the retrieved SWE from LUT and the time it takes to do a single SWE retrieval.

For satellite retrieval algorithms, there are several level products. For level 2 products, the goal is to retrieve SWE globally fast within 3 to 4 days of revisit. This means level 2 algorithms should require a minimal amount of prior and ancillary information. For higher-level products, there can be more priors for earth science applications including the use of data assimilation with land surface models. To the extent that some prior info helps to constrain the algorithm's solution space for SWE (vs. a no-prior scenario), any source of prior info could serve this function, provided we have some confidence in its quality. However, other requirements can influence which sources are ultimately feasible. For example, if the algorithm is targeting a global satellite application producing a SWE product with a horizontal spatial resolution of < 1 km, then, ideally, we would therefore need prior info at the same spatial resolution. However, global reanalysis products are typically at much coarser

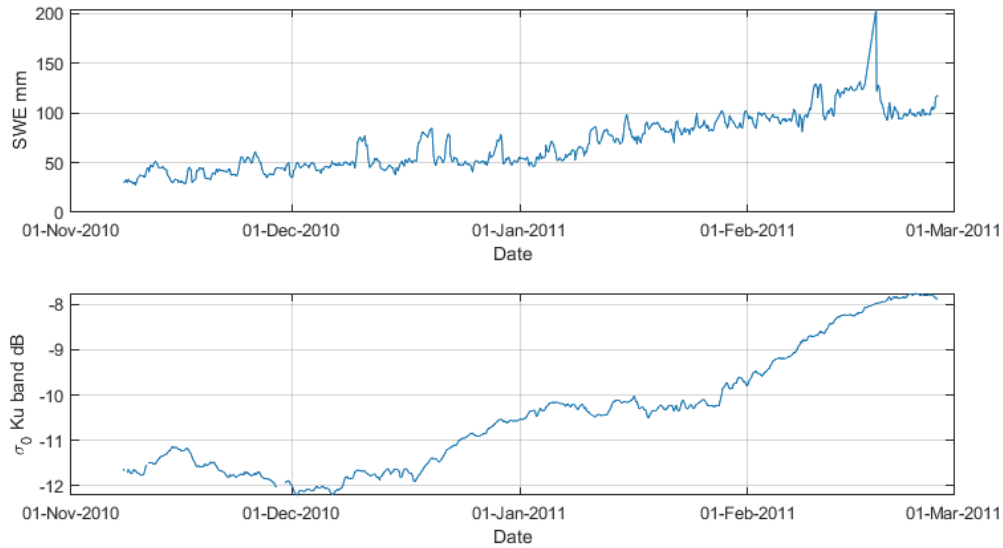


FIGURE 11. Time series data of SWE and backscatter at Ku band for NoSREx 2010–2011.

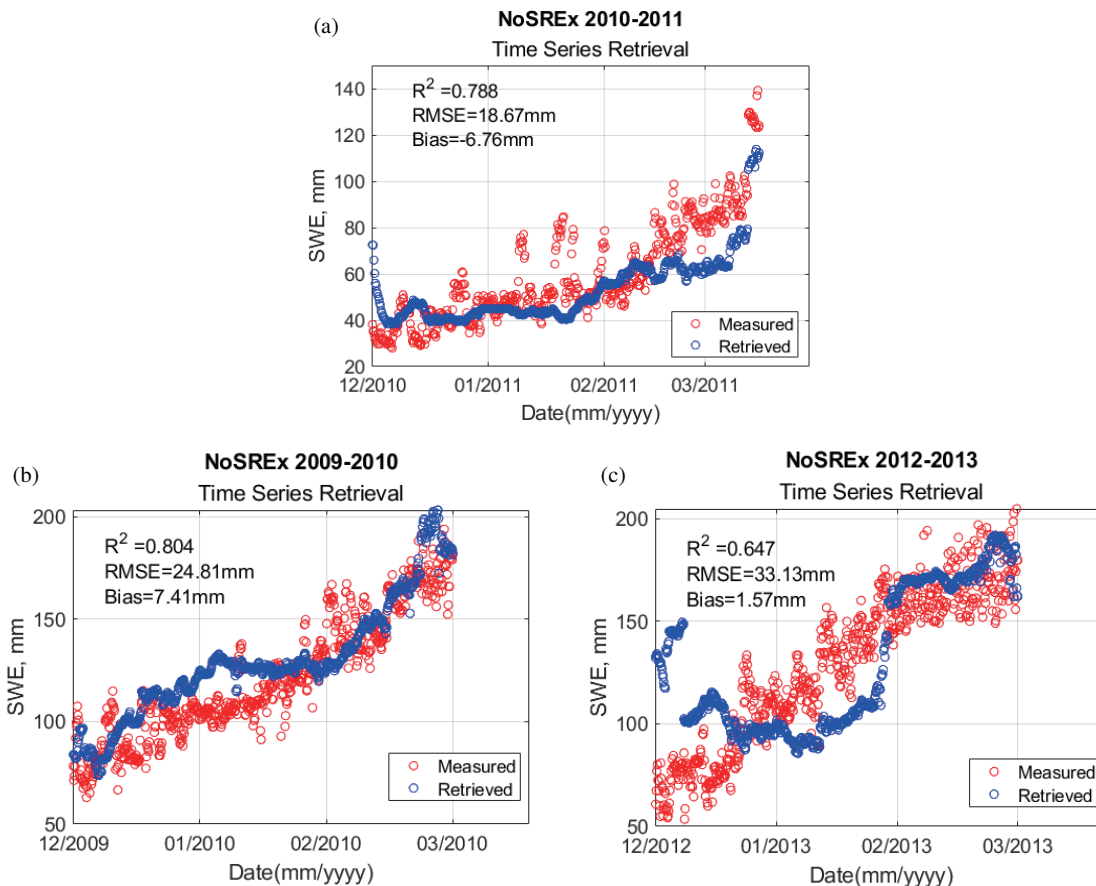


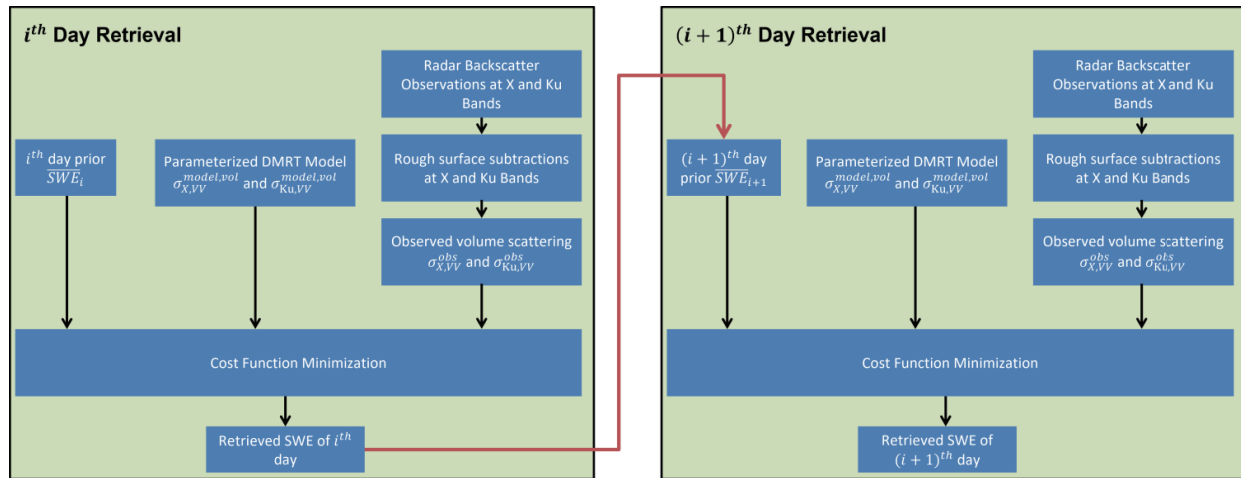
FIGURE 12. Retrieve SWE versus true SWE (in-situ measured SWE) for the time series retrieval (a) NoSREx 2010–2011, (b) NoSREx 2009–2010 and (c) NoSREx 2012–2013.

resolution. Accurately downscaling to a finer resolution would be a significant effort, greatly increasing the scope of the work needed just to obtain a prior. Other considerations include the physical difference between what a reanalysis grid cell SWE

value represents and the SWE that our algorithm is trying to estimate using real-world observations, exacerbated by the aforementioned spatial scale differences. Hence, in this paper, we do not use any reanalysis SWE product but use the previously re-

TABLE 3. Computation time for I-P-Bicon/DMRT LUT vs direct inversion.

		I-P-Bicon/DMRT LUT	Single SWE Retrieval
Finland SnowSAR 2011	Airborne	0.11 sec	0.004 sec
Finland SnowSAR 2012		0.35 sec	
TVC SnowSAR 2013		1.12 sec	
Grand Mesa SnowSAR 2017		0.26 sec	
NoSREx 2009–2010	Tower	2.2 sec	
NoSREx 2010–2011		1.89 sec	
NoSREx 2012–2013		2.4 sec	

**FIGURE 13.** Flowchart for the cost function-based retrieval algorithm.

trieved SWE as a prior as this eliminates the above-mentioned issues.

6. COST FUNCTION MINIMIZATION WITH PRIOR SWE AND NO PRIOR ON ALBEDO AND TIME SERIES PRIOR

The cost function-based approach to retrieve SWE is a constraint minimization problem, where the squared difference between the observed volume radar backscatter at X and Ku band, $\sigma_{X,VV}^{obs}$ and $\sigma_{Ku,VV}^{obs}$ respectively and the parameterized DMRT model volume backscatter at X and Ku band, $\sigma_{X,VV}^{model,vol}(SWE, \omega_X)$ and $\sigma_{Ku,VV}^{model,vol}(SWE, \omega_X)$ respectively is minimized. The cost function is guided by a prior estimate of SWE so that it doesn't fall into local minimums. Equation (10) gives the cost function.

$$F = \min_{\omega_X, SWE} \left\{ \begin{aligned} & \frac{w_1}{2s_X^2} \left(\sigma_{X,VV}^{obs} - \sigma_{X,VV}^{model,vol}(SWE, \omega_X) \right)^2 \\ & + \frac{w_2}{2s_{Ku}^2} \left(\sigma_{Ku,VV}^{obs} - \sigma_{Ku,VV}^{model,vol}(SWE, \omega_X) \right)^2 \\ & + \frac{w_3}{2s_{SWE}^2} (SWE - \bar{SWE})^2 \end{aligned} \right\} \quad (10)$$

The w_1 , w_2 , and w_3 are weights of each term in the cost function. s_X , and s_{Ku} are the uncertainties, i.e., the standard deviation of the radar measurements at X- and Ku-band, respectively,

where s_{SWE} acts as the uncertainty or the standard deviation of SWE. The retrieval is done based on time series. For the first retrieval of the season, we set $\bar{SWE} = 50$ mm and find the retrieved SWE. Then, going to the second day, we use the first day's retrieved SWE and set that as the prior \bar{SWE} for the second day. We repeat this for the entire season by setting the current day's \bar{SWE} as the previous day's retrieved SWE till the end of the dry snowfall season. There is no prior on grain size or scattering albedo in this cost function algorithm. This is described in the flowchart in Figure 13.

The NoSREx 2010–2011 data as described in Section 5 is used to validate the cost function-based algorithm. The weights w_1 , w_2 , and w_3 are all set to unity. The radar observation uncertainties are set to 0.5 dB ($s_X = s_{Ku} = 0.5$ dB) and the uncertainty in SWE is set to 30 mm ($s_{SWE} = 30$ mm). Using these parameters and minimizing the volume radar backscatter of the NoSREx data, we achieve a retrieval performance as shown in Figure 14.

The retrieval shown in Figure 14 is one of many possible solutions of the cost function as it is solving a minimization problem on the parameterized DMRT model. As opposed to the algebraic inversion method, in which we solve the model exactly and hence only have two solutions. These many possible solutions depend on the weights and uncertainties in the cost function and are sometimes difficult to find as the statistics

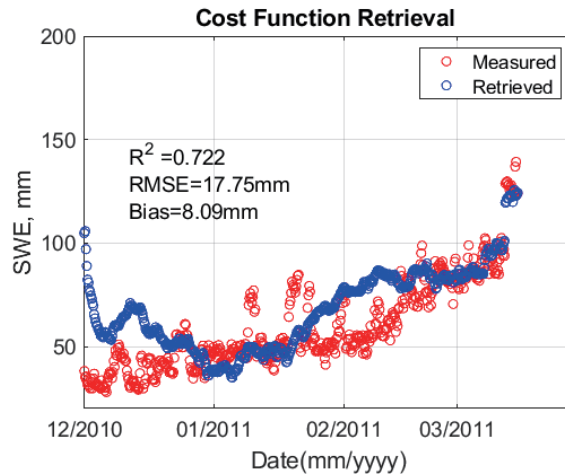


FIGURE 14. Retrieval result for NoSREx 2010–2011 using cost function-based approach.

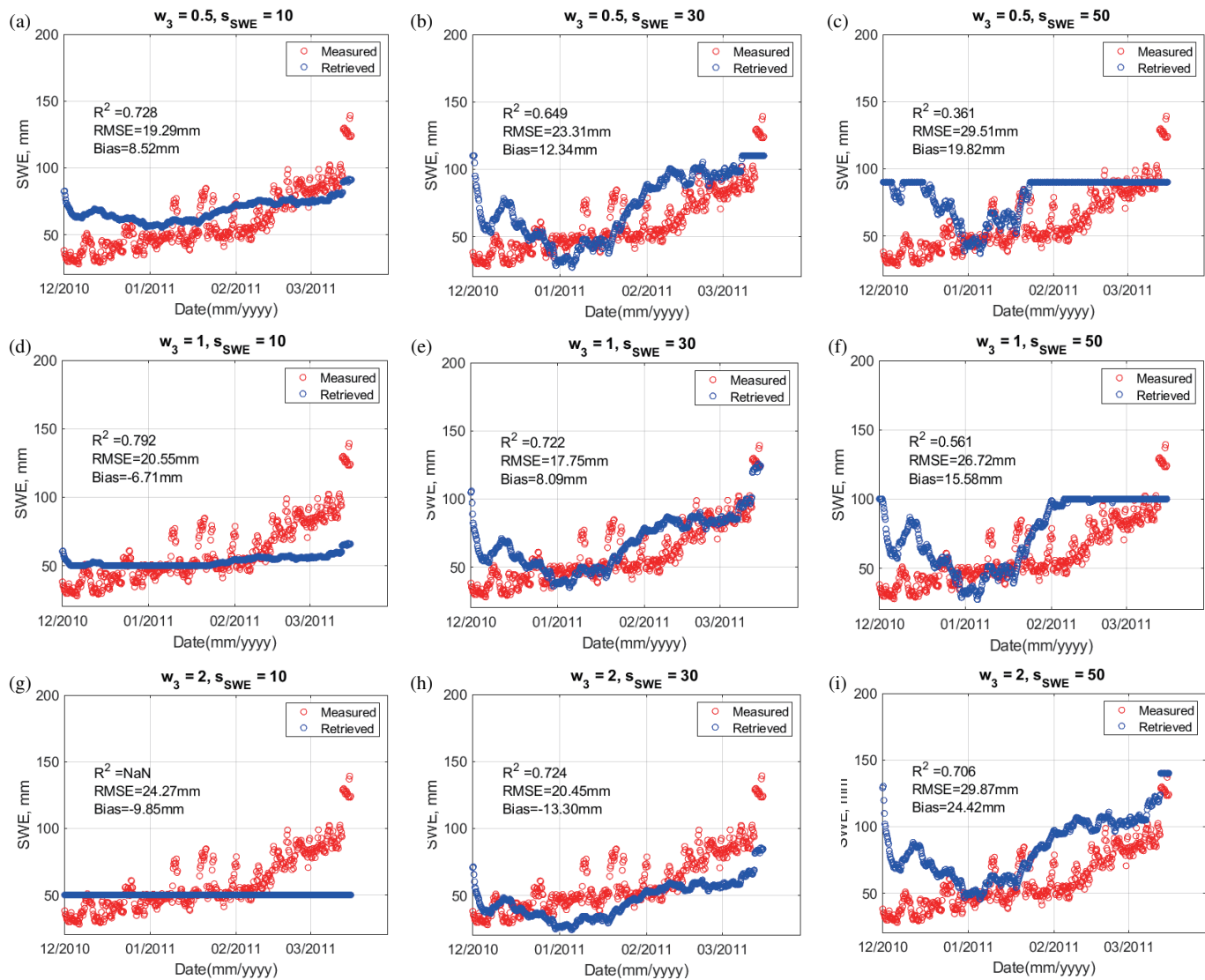


FIGURE 15. Different answers for retrieved SWE for different combinations of w_3 and s_{SWE} . (a), (b) and (c) correspond to $w_3 = 0.5$ and $s_{SWE} = 10, 30$ and 50 . (d), (e) and (f) correspond to $w_3 = 1$ and $s_{SWE} = 10, 30$ and 50 and (g), (h) and (i) correspond to $w_3 = 2$ and $s_{SWE} = 10, 30$ and 50 .

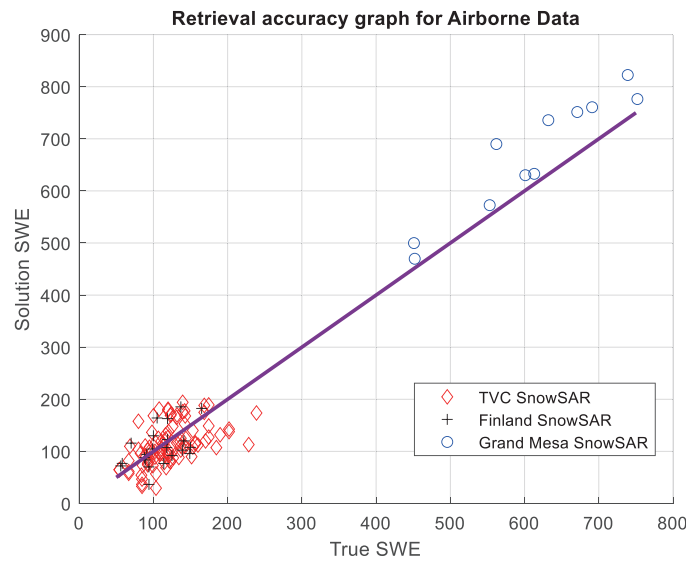


FIGURE 16. SWE retrieval accuracy graph for all the airborne data.

TABLE 4. RMSE of retrieved SWE for different combinations of w_3 and s_{SWE} .

	$s_{SWE} = 10$	$s_{SWE} = 30$	$s_{SWE} = 50$
$w_3 = 05$	19.29	23.31	29.51
$w_3 = 1$	20.55	17.75	26.72
$w_3 = 2$	24.27	20.45	29.87

of these uncertainties are not known due to a lack of a robust dataset. This can result in varying answers of retrieved SWE with different RMSE all depending upon the choice of these weights and uncertainties. This is illustrated in Figure 15 which shows the different answers of SWE one can get by changing the cost function parameters. These results are obtained by keeping $w_1 = w_2 = 1$ and $s_X = s_{Ku} = 0.5$ dB and varying w_3 as 0.5, 1 and 2. s_{SWE} is varied to 10, 30 and 50 mm.

We can see that when the uncertainty in SWE is small ($s_{SWE} = 10$ mm), the retrieved SWE has very little variations for all the weights of w_3 . The cost function finds answers close to the first retrieved result and gives a much flatter response as shown in Figures 15(a), (d), and (g). When the s_{SWE} is increased to 30 and 50, there are more variations in the SWE answer as the cost function can find SWE values that are farther from the first retrieved SWE. The different variations of s_{SWE} and w_3 resulted in different answers of retrieved SWE with different RMSE as shown in Table 4. Numbers in Table 4 correspond to RMSE of different combinations of w_3 and s_{SWE} . Statical data is needed to be available to obtain the optimal weights of variances.

In the cost function-based approach, these errors and uncertainties can be included which should provide a more accurate retrieval. But the challenge is to get these parameters of uncertainties and weights correctly, where currently lies the drawback of a cost function minimization-based approach. In the future, with a large amount of satellite observed data, in combination with ground truth measurements at particular locations,

we can create an accurate statistical model for the observed SWE and find the standard deviation associated with it. Current ground truth data are not spatially or temporally varied enough to get these accurate statistics. The standard deviation associated with the radar backscatter measurement is a property of the instrument itself and can be known. In the case of the NoSREx data, the optimal weight and SWE variance did not vary over the three years, as shown in [40] as it was only a single location of time series data and the total SWE for the three years was less than 200 mm.

7. COMPARISONS OF 3 ALGORITHMS

For satellite missions, we will use time series as the basis for prior SWE. In Table 5, we give a table of comparisons of results using the tower time series data. The comparisons are the algebraic algorithm, the cost function with best performance, and the Zhu et al. algorithm.

Zhu et al. algorithm put the prior on albedo and no prior on SWE. Although Zhu et al. use the “true SWE” to decide on the prior albedo, the albedo Zhu et al. picked is the “quite wrong albedo” that differs from the true albedo by 50%, and Zhu et al.’s algorithm still has good performance despite “quite wrong prior albedo”. This can be seen in the table as both the cost function-based approach of this paper and Zhu et al. retrieval have comparable performance.

Table 6 shows the prior, weights and error variance used in the two approaches discussed in the paper. The weight and error

TABLE 5. Comparison of three algorithms for the three years of NoSREx data.

	Algebraic Inversion	Cost Function (Optimal weights and variances)	Zhu et al. retrieval
NoSREx 2009–2010	24.81 mm	24.22 mm	26.30 mm
NoSREx 2010–2011	18.67 mm	17.75 mm	17.05 mm
NoSREx 2012–2013	33.13 mm	30.04 mm	31.71 mm

TABLE 6. Prior SWE, weights, and error variances for the two algorithms.

Data	Approach	Prior SWE	Weight	Error variance
Airborne data	Algebraic approach	75% different from true SWE	None	None
Tower time series data	Algebraic approach	Prior SWE starts with zero, then SWE of the previous day	None	None
Tower time series data	Cost function approach	Prior SWE starts with 50 mm, then SWE of the previous day	$w_3 = 1$	$s_{SWE} = 30$

variance of the cost function approach is the one used to achieve optimal performance.

8. SUMMARY AND DISCUSSIONS

In this paper, we developed fast SWE retrieval algorithms that combined with time series do not require any ancillary information. The volume scattering approach of the X band and Ku band has been criticized for the large amount of required ancillary information. For level 2 products, unlike level 4 products, ancillary information is undesirable.

We developed a fast algebraic inversion-based algorithm to retrieve SWE using the parameterized Bic-DMRT model and the inverse parametrized Bic-DMRT LUT and a cost function minimization-based retrieval with prior on SWE. This algebraic inversion algorithm directly gives the SWE from the measured backscattering of sigma X and sigma Ku. We show that there are at most two possible solutions of SWE for a given pair of volume backscattered observations at the X and Ku bands. The correct solution from the I-P-Bic-DMRT LUT is picked by using a very coarse prior on SWE. In the case of the airborne data, to validate the algorithm, we use a prior SWE which is 75% different from true SWE and for the time series-based retrieval, we use the previous day's retrieved SWE as a prior for the current day's retrieval. Using these priors, we achieve satisfactory performance when validating the algorithm against airborne and tower-based data. In the future for satellite data, we will use the time series approach. The advantage of both the algebraic inversion and cost function algorithm, compared to previous dual frequency-based algorithms, such as CoReH₂O is that there is no prior on grain size or scattering albedo or any other hard to get snow microstructure property.

Figure 16 shows the retrieval accuracy of the algorithm by plotting all the retrieved results in the same plot. The algorithm was able to retrieve SWE within some error for both the low range of SWE (50 to 250 mm) and the very high range of SWE (450 mm to 750 mm). There is a lack of data for the gap region of the middle ranges of SWE between 250 mm and 350 mm. But current and future NASA SnowEx campaigns hope to fill this gap. Once those data are available, this algorithm will be validated against those data so that we have a full range of SWE retrieval.

The algorithm also can be improved in the future. There can be more robust training of the Bic-DMRT model to give a better parameterized model for various SWE ranges and various snow conditions in various regions of the world. There can be a library of parametrized Bic-DMRT together with the I-P-Bic-DMRT LUT. The algorithm is currently based on a single-layer model. The effects of layering and ice crusts on the backscattered signal also need to be studied in the future. Currently, there has been a new proposal for a satellite mission for global SWE retrieval using dual frequency X and Ku band radar. The baseline algorithm for the proposal is a cost function-based algorithm outlined in [40], which uses a prior on ω_X .

ACKNOWLEDGEMENT

The research at University of Michigan, Ann Arbor was supported in part by the National Aeronautics and Space Administration's (NASA) Terrestrial Hydrology Program (THP) for the SnowEx measurements and in part by the Instrument Incubator Program (IIP).

REFERENCES

- [1] Zhu, J., S. Tan, J. King, C. Derksen, J. Lemmetyinen, and L. Tsang, "Forward and inverse radar modeling of terrestrial snow using snowSAR data," *IEEE Transactions on Geoscience and Remote Sensing*, Vol. 56, No. 12, 7122–7132, 2018.
- [2] Zhu, J., S. Tan, L. Tsang, D.-H. Kang, and E. Kim, "Snow water equivalent retrieval using active and passive microwave observations," *Water Resources Research*, Vol. 57, No. 7, 2021.
- [3] Rott, H., S. H. Yueh, D. W. Cline, C. Duguay, R. Essery, C. Haas, F. Heliere, M. Kern, G. Macelloni, E. Malnes, T. Nagler, J. Pulliainen, H. Rebhan, and A. Thompson, "Cold regions hydrology high-resolution observatory for snow and cold land processes," *Proceedings of The IEEE*, Vol. 98, No. 5, 752–765, May 2010.
- [4] Tsang, L., M. Durand, C. Derksen, A. P. Barros, D.-H. Kang, H. Lievens, H.-P. Marshall, J. Zhu, J. Johnson, J. King, J. Lemmetyinen, M. Sandells, N. Rutter, P. Siqueira, A. Nolin, B. Osmanoglu, C. Vuyovich, E. Kim, D. Taylor, I. Merkouriadi, L. Brucker, M. Navari, M. Dumont, R. Kelly, R. S. Kim, T.-H. Liao, F. Borah, and X. Xu, "Review article: global monitoring of snow water equivalent using high-frequency radar remote sensing," *Cryosphere*, Vol. 16, No. 9, 3531–3573, Sep. 2022.
- [5] Shi, J., "Snow water equivalence retrieval using X and Ku band dual-polarization radar," in *2006 IEEE International Symposium on Geoscience and Remote Sensing*, 2183–2185, 2006.
- [6] Yueh, S. H., S. J. Dinardo, A. Akgiray, R. West, D. W. Cline, and K. Elder, "Airborne Ku-band polarimetric radar remote sensing of terrestrial snow cover," *IEEE Transactions on Geoscience and Remote Sensing*, Vol. 47, No. 10, 3347–3364, 2009.
- [7] Chang, A. T. C., J. L. Foster, D. K. Hall, A. Rango, and B. K. Hartline, "Snow water equivalent estimation by microwave radiometry," *Cold Regions Science and Technology*, Vol. 5, No. 3, 259–267, 1982.
- [8] Chang, A. T. C., J. L. Foster, M. Owe, D. K. Hall, and A. Rango, "Passive and active microwave studies of wet snowpack properties: results of March 4, 1981, aircraft mission," *Hydrology Research*, Vol. 16, No. 2, 57–66, 1985.
- [9] Tsang, L., C.-T. Chen, A. T. Chang, J. Guo, and K.-H. Ding, "Dense media radiative transfer theory based on quasicrystalline approximation with applications to passive microwave remote sensing of snow," *Radio Science*, Vol. 35, No. 3, 731–749, 2000.
- [10] Kelly, R. E., A. T. Chang, L. Tsang, and J. L. Foster, "A prototype AMSR-E global snow area and snow depth algorithm," *IEEE Transactions on Geoscience and Remote Sensing*, Vol. 41, No. 2, 230–242, 2003.
- [11] Foster, J. L., C. Sun, J. P. Walker, R. Kelly, A. Chang, J. Dong, and H. Powell, "Quantifying the uncertainty in passive microwave snow water equivalent observations," *Remote Sensing of Environment*, Vol. 94, No. 2, 187–203, 2005.
- [12] Zuniga, M. A., T. M. Habashy, and J. A. Kong, "Active remote sensing of layered random media," *IEEE Transactions on Geoscience Electronics*, Vol. 17, No. 4, 296–302, 1979.
- [13] Ulaby, F. T. and W. H. Stiles, "The active and passive microwave response to snow parameters: 2. water equivalent of dry snow," *Journal of Geophysical Research: Oceans*, Vol. 85, No. C2, 1045–1049, 1980.
- [14] Tsang, L., J. Pan, D. Liang, Z. Li, D. W. Cline, and Y. Tan, "Modeling active microwave remote sensing of snow using dense media radiative transfer (DMRT) theory with multiple-scattering effects," *IEEE Transactions on Geoscience and Remote Sensing*, Vol. 45, No. 4, 990–1004, 2007.
- [15] Proksch, M., C. Mätzler, A. Wiesmann, *et al.*, "MEMLS3&a: microwave emission model of layered snowpacks adapted to include backscattering," *Geosci Model Dev*, Vol. 8, No. 8, 2611–2626, 2015.
- [16] Xu, X., L. Tsang, and S. Yueh, "Electromagnetic models of co/cross polarization of bicontinuous/dmrt in radar remote sensing of terrestrial snow at X-and Ku-band for CoReH₂O and SCLP applications," *IEEE Journal of Selected Topics in Applied Earth Observations and Remote Sensing*, Vol. 5, No. 3, 1024–1032, 2012.
- [17] Tan, S., W. Chang, L. Tsang, J. Lemmetyinen, and M. Proksch, "Modeling both active and passive microwave remote sensing of snow using dense media radiative transfer (DMRT) theory with multiple scattering and backscattering enhancement," *IEEE Journal of Selected Topics in Applied Earth Observations and Remote Sensing*, Vol. 8, No. 9, 4418–4430, 2015.
- [18] Picard, G., M. Sandells, and H. Löwe, "SMRT: An active-passive microwave radiative transfer model for snow with multiple microstructure and scattering formulations (v1.0)," *Geosci Model Dev*, Vol. 11, No. 7, 2763–2788, Jul. 2018.
- [19] Lemmetyinen, J., C. Derksen, H. Rott, *et al.*, "Retrieval of effective correlation length and snow water equivalent from radar and passive microwave measurements," *Remote Sens (Basel)*, Vol. 10, No. 2, 170, Jan. 2018.
- [20] King, J., C. Derksen, P. Toose, A. Langlois, C. Larsen, J. Lemmetyinen, P. Marsh, B. Montpetit, A. Roy, N. Rutter *et al.*, "The influence of snow microstructure on dual-frequency radar measurements in a tundra environment," *Remote Sensing of Environment*, Vol. 215, 242–254, 2018.
- [21] Kuga, Y. and A. Ishimaru, "Retroreflectance from a dense distribution of spherical particles," *Journal of the Optical Society of America A*, Vol. 1, No. 8, 831–835, 1984.
- [22] Tsang, L. and A. Ishimaru, "Backscattering enhancement of random discrete scatterers," *Journal of the Optical Society of America A*, Vol. 1, No. 8, 836, 1984.
- [23] Tsang, L. and J. A. Kong, *Scattering of Electromagnetic Waves: Advanced Topics*, John Wiley & Sons, 2004.
- [24] Cui, Y., C. Xiong, J. Lemmetyinen, J. Shi, L. Jiang, B. Peng, H. Li, T. Zhao, D. Ji, and T. Hu, "Estimating snow water equivalent with backscattering at X and Ku band based on absorption loss," *Remote Sensing*, Vol. 8, No. 6, 505, 2016.
- [25] Xiong, C., J. Shi, and J. Lemmetyinen, "Refinement of the X and Ku band dual-polarization scatterometer snow water equivalent retrieval algorithm," in *2014 IEEE Geoscience and Remote Sensing Symposium*, 2419–2422, 2014.
- [26] Xiong, C. and J. Shi, "The potential for estimating snow depth with quikscat data and a snow physical model," *IEEE Geoscience and Remote Sensing Letters*, Vol. 14, No. 7, 1156–1160, 2017.
- [27] Santi, E., S. Paloscia, S. Pettinato, L. D. Gregorio, G. Cuzzo, A. Jacob, C. Notarnicola, F. Cigna, and D. Tapete, "SWE retrieval in alpine areas with high-resolution cosmo-skymed X-band SAR data using artificial neural networks and support vector regression techniques," in *2020 Xxxiiird General Assembly and Scientific Symposium of The International Union of Radio Science*, 1–4, 2020.
- [28] Sensing, P. M. R., "Inversion of snow parameters from passive microwave remote sensing measurements by a neural network trained with a multiple scattering model," *IEEE Transactions on Geoscience and Remote Sensing*, Vol. 30, No. 5, 1015, 1992.
- [29] Chang, A. T. C. and L. Tsang, "A neural network approach to inversion of snow water equivalent from passive microwave measurements," *Hydrology Research*, Vol. 23, No. 3, 173–182, 1992.
- [30] Du, J., J. Shi, and H. Rott, "Comparison between a multiple-scattering and multi-layer snow scattering model and its param-

- eterized snow backscattering model,” *Remote Sensing of Environment*, Vol. 114, No. 5, 1089–1098, 2010.
- [31] Oh, Y., K. Sarabandi, and F. T. Ulaby, “An empirical model and an inversion technique for radar scattering from bare soil surfaces,” *IEEE Transactions on Geoscience and Remote Sensing*, Vol. 30, No. 2, 370–381, 1992.
- [32] Zhu, J., L. Tsang, T.-H. Liao, J. T. Johnson, D. H. Kang, and E. J. Kim, “Radar backscattering of rough soil surfaces from L-band to Ku-band with NMM3D,” *IEEE Geoscience and Remote Sensing Letters*, Vol. 19, 1–5, 2022.
- [33] Ding, K.-H., X. Xu, and L. Tsang, “Electromagnetic scattering by bicontinuous random microstructures with discrete permittivities,” *IEEE Transactions on Geoscience and Remote Sensing*, Vol. 48, No. 8, 3139–3151, 2010.
- [34] Mätzler, C., “Improved born approximation for scattering of radiation in a granular medium,” *J. Appl. Phys.*, Vol. 83, No. 11, 6111–6117, Jun. 1998.
- [35] Mätzler, C., “Relation between grain-size and correlation length of snow,” *Journal of Glaciology*, Vol. 48, No. 162, 461–466, Sep. 2002.
- [36] Lemmetyinen, J., J. Pulliainen, A. Rees, A. Kontu, Y. Qiu, and C. Derksen, “Multiple-layer adaptation of hut snow emission model: comparison with experimental data,” *IEEE Transactions on Geoscience and Remote Sensing*, Vol. 48, No. 7, 2781–2794, 2010.
- [37] Pan, J., M. Durand, M. Sandells, J. Lemmetyinen, E. J. Kim, J. Pulliainen, A. Kontu, and C. Derksen, “Differences between the HUT snow emission model and MEMLS and their effects on brightness temperature simulation,” *IEEE Transactions on Geoscience and Remote Sensing*, Vol. 54, No. 4, 2001–2019, 2015.
- [38] Lemmetyinen, J., J. Cohen, A. Kontu, *et al.*, “Airborne snowsar data at X and Ku bands over boreal forest, alpine and tundra snow cover,” *Earth Syst. Sci. Data*, Vol. 14, No. 9, 3915–3945, Sep. 2022.
- [39] Lemmetyinen, J., A. Kontu, J. Pulliainen, *et al.*, “Nordic snow radar experiment,” *Geoscientific Instrumentation, Methods and Data Systems*, Vol. 5, No. 2, 403–415, Sep. 2016.
- [40] Durand, M., J. T. Johnson, J. Dechow, L. Tsang, F. Borah, and E. J. Kim, “Retrieval of SWE from dual-frequency radar measurements: Using timeseries to overcome the need for accurate a priori information,” *Egusphere*, Vol. 2023, 1–23, 2023.